

## Duplex Mikaelian and Duplex Maxwell's Fish-Eye Lenses

Huiyan Peng<sup>1,2,3</sup> Senlin Liu<sup>1,2</sup> Yuze Wu<sup>1,2</sup> Yi Yan<sup>1,2</sup> Zichun Zhou<sup>1,2</sup> Xiaochao Li,<sup>1,2</sup>  
Qiaoliang Bao,<sup>4</sup> Lin Xu<sup>1,3,†</sup> and Huanyang Chen<sup>1,2,\*</sup>

<sup>1</sup>*Institute of Electromagnetics and Acoustics and Key Laboratory of Electromagnetic Wave Science and Detection Technology, Xiamen University, Xiamen 361005, China*

<sup>2</sup>*Department of Electrical and Electronics Engineering, Xiamen University Malaysia, 43900 Sepang, Selangor, Malaysia*

<sup>3</sup>*Institutes of Physical Science and Information Technology and Key Laboratory of Opto-Electronic Information Acquisition and Manipulation of Ministry of Education, Anhui University, Hefei 230601, China*

<sup>4</sup>*Department of Materials Science and Engineering, and ARC Centre of Excellence in Future Low-Energy Electronics Technologies (FLEET), Monash University, Clayton, Victoria 3800, Australia*

(Received 16 October 2019; revised manuscript received 28 December 2019; accepted 3 March 2020; published 19 March 2020)

Here, we report two kinds of absolute optical instruments that can make stigmatic images for geometric optics in two-dimensional space. One is called the duplex Mikaelian lens, which is made by splicing two half-Mikaelian lenses with different periods. The other is an exponential conformal transformer of a duplex Mikaelian lens with a rational number of the ratio of different periods of its two half-Mikaelian lenses, which we call a duplex Maxwell's fish-eye lens. Duplex Mikaelian lenses have continuous translation symmetry with an arbitrary real number, while duplex Maxwell's fish-eye lenses have continuous rotation symmetry from zero to  $2\pi$ . Hence, each duplex Maxwell's fish-eye lens corresponds to a duplex Mikaelian lens. We further demonstrate the caustic effect of geometric optics in duplex Mikaelian lenses and duplex Maxwell's fish-eye lenses. In addition, we investigate the Talbot effect of wave optics in the duplex Mikaelian lens based on numeric calculations. Our findings, based on splicing and exponential conformal mapping, enlarge the family of absolute optical instruments.

DOI: 10.1103/PhysRevApplied.13.034050

### I. INTRODUCTION

Recently, absolute optical instruments (AOIs) [1–7] that can make stigmatic images in geometrical optics have drawn much attention, such as Maxwell's fish-eye lens [1], the Luneburg lens [3], and the Miñano lens [4]. They are widely used in different areas, such as subwavelength focusing [8–10] and transformation optical designs [11–13]. A two-dimensional (2D) AOI with a gradient refractive index of rotation symmetry can be cast into another 2D AOI with a gradient refractive index of continuous translation symmetry by exponential conformal mapping,  $w = \exp(z)$ . The well-studied example is the pairing of a Maxwell's fish-eye lens and a Mikaelian lens [14]. The gradient refractive index of a Mikaelian lens is written as  $1/\cosh(x)$  [15]. In addition to continuous translation symmetry along the  $y$  axis, the Mikaelian lens has discrete mirror symmetry of the  $y$  axis. Self-focusing

of geometrical optics and the Talbot effect of wave phenomena in the Mikaelian lens had been investigated both theoretically and experimentally [14].

Here, we construct two kinds of AOIs. One is made by splicing two half-Mikaelian lenses with different periods, which we call the duplex Mikaelian lens. The duplex Mikaelian lens has continuous translation symmetry in one direction without mirror symmetry in another direction. By exponential conformal mapping, the duplex Mikaelian lens with a rational number as the ratio of different periods of its two half-Mikaelian lenses can be cast into another kind of AOI with continuous rotation symmetry, which we call the duplex Maxwell's fish-eye lens. This paper is organized as follows. In Sec II, we introduce Mikaelian lenses and their exponential conformal transformers. In Sec. III, we construct the duplex Mikaelian lens and the duplex Maxwell's fish-eye lens. In Sec. IV, we demonstrate the caustic effect of geometric optics in duplex Mikaelian lenses and duplex Maxwell's fish-eye lenses. In Sec. V, the Talbot effect of wave optics in the duplex Mikaelian lens is illustrated based on numeric calculations. In Sec. VI, we give a conclusion.

†xuin@ahu.edu.cn

\*kenyon@xmu.edu.cn

## II. MIKAELIAN LENSES AND THEIR EXPONENTIAL CONFORMAL TRANSFORMERS

In general, the Mikaelian lens in two-dimensional space can be expressed as

$$n(x) = 1/\cosh(px/a), \quad (1)$$

where  $a$  is a reference scale length and  $p$  is a positive real number. In principle, we can absorb  $p$  into  $a$  and redefine  $a/p$  as  $a'$ ; therefore, the  $p$  term can be removed from Eq. (1). However, for the following discussion of exponential conformal mapping, we call the lens with a gradient refractive index satisfying Eq. (1) the Mikaelian lens, with  $\{p\}$ . The continuous translation symmetry of Eq. (1) is of the one-dimensional Lie group  $R^1$ , namely, real numbers, which is noncompact. The light rays marked with red and blue lines from a red point source with the position coordinate  $(0, 0)$  can result in self-focusing; see the red and blue points with the interval  $\pi a/2$  along the  $y$  axis in Fig. 1(a) with  $p = 2$ . As illustrated in Fig. 1(a), during

the reference period length  $L = 2\pi a$  between two horizontal dashed lines, we have two periods for the Mikaelian lens with a refractive index written as Eq. (1). Hence, it is a Mikaelian lens with a period length of  $L_0 = L/p$ , where light rays travel periodically. The light trajectories in the Mikaelian lens are expressed by  $k \sinh(x/a) = \sin(y/a)$  [15], where  $k$  is the slope of the light ray at the red point source with the position coordinate  $(0, 0)$ . Here, we perform ray-tracing calculations based on the Hamiltonian equation of optics [16].

Now, let us revisit the exponential conformal mapping [14], which is written as

$$w/a = \exp(z/a), \quad z/a = \log(|w/a|) + [\arg(w/a) + 2j\pi]i, \quad (2)$$

where  $j$  is an integer. It connects a Riemann surface, as shown by the chiral rotated surface (denoted with  $w = u + vi$ ) in Fig. 1(b), to a complex plane (denoted with  $z = x + yi$ ) in Fig. 1(a). The chiral rotated surface is the schematic plot of the Riemann surface, which looks like the wave

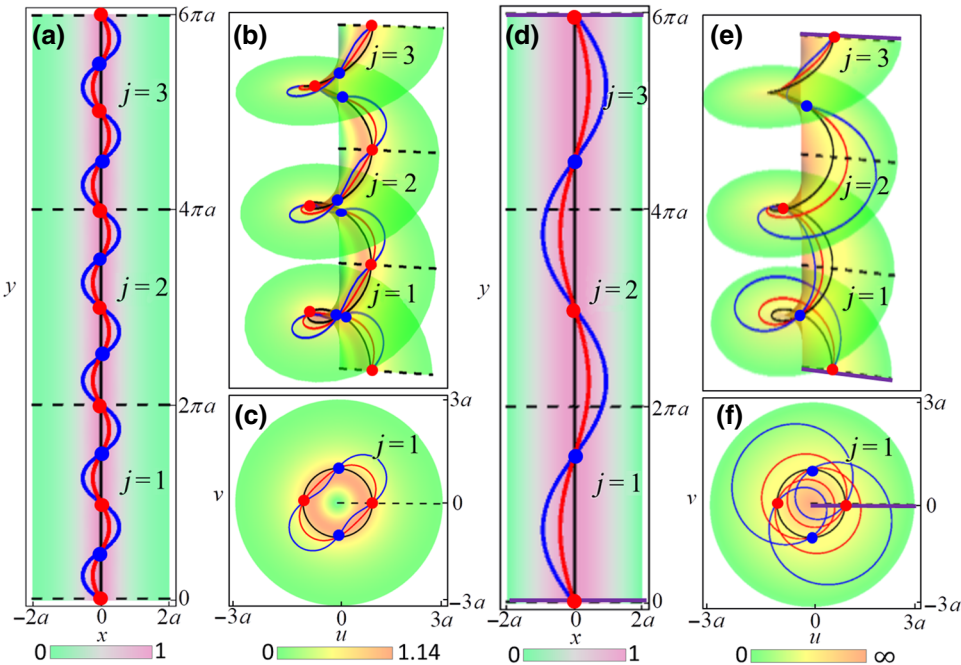


FIG. 1. Gradient refractive index and light trajectories in the Mikaelian lens  $|E_z|$  and the corresponding Maxwell's fish-eye lens. (a) Mikaelian lens with  $\{p = 2\}$  is in  $z$  space, which is divided into infinite number ribbon regions (marked with integer  $j$ ), with a reference period length  $L = 2\pi a$  between dashed lines. Its gradient refractive index, written as Eq. (1), is shown with the contour plot in complex plane  $z = x + yi$ . Two red and blue light rays launch from the red source at position coordinate  $(0, 0)$ . In the reference period length, the red source can make three more images marked with two blue points and a red point. (b) Schematic plot of the Riemann surface of exponential conformal mapping. Branch cuts are denoted by dashed lines, which are mapped from the dashed lines of  $z$  space. Chiral rotated surface is used to lift a third space dimension for a better illustration of branch cuts. (c) Corresponding gradient refractive index and light trajectories in the Maxwell's fish-eye lens, which is mapped from the ribbon region marked with  $j = 1$  of the part "a" figure by exponential conformal mapping. Indeed, it is also the projection from multiple  $w$  space of the Riemann surface of (b). Radius  $a$  denoted with a black circle is mapped from the  $y$  axis of  $z$  space. (d) Mikaelian lens with  $\{p = 2/3\}$  is in  $z$  space. Two additional purple lines denote boundaries of the large period. (e) Light rays in the Riemann surface of Maxwell's fish-eye lens with  $\{p = 2/3\}$ . (f) Light rays in Maxwell's fish-eye lens with  $\{p = 2/3\}$ .

front of right circular polarized light. Each region (marked with  $j$ ) between dashed lines is indeed a plane with a branch cut (see the dashed line), as shown in Fig. 1(c). Here, we use the chiral rotated surface to lift the third space dimension for a better illustration of branch cuts, which will be useful for further discussion. One important thing is that each ribbon region between dashed lines marked with integer  $j$  in Fig. 1(a) has a reference period length  $L = 2\pi a$ , which corresponds to a complex plane. The  $y$  axis, denoted by the black line in Fig. 1(a), is mapped to a spiral black curve in Fig. 1(b), and hence, corresponding to the black circle in Fig. 1(c). According to conformal transformation optics [11,17], the gradient refractive index between  $z$  space and  $w$  space can be expressed by

$$n(w) = |dz/dw|n(z), \quad (3)$$

where  $n(z)$  and  $n(w)$  are the gradient refractive indexes of  $z$  space and  $w$  space respectively. Hence, the gradient refractive index  $n(z) = n(x + yi) = n(x)$  in Eq. (1) of the Mikaelian lens with  $\{p\}$  in  $z$  space can be cast into a gradient refractive index in  $w$  space with the form of

$$n(w) = 2/[abs(w/a)^{1+p} + abs(w/a)^{1-p}], \quad (4)$$

the continuous rotation symmetry of which is of another one-dimensional Lie group  $S^1$ , namely, a circle group from zero to  $2\pi$ , which is compact compared with the Lie group  $R^1$ . When  $p$  is a rational number, Eq. (4) denotes the gradient refractive index of the generalized Maxwell's fish-eye lens [18], which we call the Maxwell's fish-eye lens with  $\{p\}$ . The conventional Maxwell's fish-eye lens refers to Maxwell's fish-eye lens with  $\{p = 1\}$ , which is an AOI in optics as a purely geometrical device [5]. The light rays in such a Maxwell's fish-eye lens with  $\{p\}$  are all closed, as shown in an example with blue and red curves in Fig. 1(c). The red point source at position coordinate  $(1, 0)$  can make another three images in the Maxwell's fish-eye lens with  $\{p = 2\}$ . The corresponding trajectories are shown in blue and red spiral curves of light rays in the Riemann surface in Fig. 1(b). As also shown in Fig. 3(d), a point source in the Maxwell's fish-eye lens with  $\{p = 1\}$  has only one image.

The Mikaelian lens with any positive real number  $\{p\}$  in Eq. (1) represents an AOI, the period length of which is  $L_0 = L/p$ . After exponential conformal mapping, we obtain a lens with the gradient refractive index defined by Eq. (4). Why can only  $p$  as a rational number in the Maxwell's fish-eye lens make it an AOI? We give a heuristic discussion based on its corresponding Mikaelian lens by exponential conformal mapping, as given by Eq. (2). Suppose that the rational number of the Maxwell's fish-eye lens with  $\{p\}$  can be denoted by  $p = p_u/p_d$ , where  $p_u$  and  $p_d$  are coprime. Now, its corresponding Mikaelian lens has a period length of  $L_0 = Lp_d/p_u$ . In this case, we can always find a large period  $L_g = Lp_d = L_0p_u$ , which is  $p_d$

times the reference period length  $L$  and  $p_u$  times the period length  $L_0$  of the Mikaelian lens. Therefore, in the region of large period  $L_g$ , light rays from one point source have  $p_d$  periods (or  $2p_d$  focusing points) in the Mikaelian lens, which correspond to winding around the original point of the Maxwell's fish-eye lens  $p_u$  times and then recovering to the original propagation condition. For certainty, we plot a Mikaelian lens with  $\{p_u/p_d = 2/3\}$  in Fig. 1(d) and its corresponding Maxwell's fish-eye lens in Fig. 1(f). As we can see, light rays from one red point source have two periods (or 4 focusing points) in the Mikaelian lens of Fig. 1(d) during the large period  $L_g = 3L$  between two purple solid lines. In the corresponding Riemann surface of Fig. 1(e), light rays can wind around the central axis three times and then make a perfect image. When we consider light rays in the real Maxwell's fish-eye lens in Fig. 1(f) projected from the Riemann surface, there is still perfect imaging. Once  $p$  is not a rational number, there is no way to find a large period, or to say the large period is infinite. Hence, light rays will wind around the central axis an infinite number of times without recovering their original propagation condition, which means that the Maxwell's fish-eye lens with an irrational number index is not an AOI. However, we know that the Mikaelian lens with any positive real number index is an AOI that can be self-focusing. The difference comes from the Lie group  $R^1$  of the Mikaelian lens and the Lie group  $S^1$  of the Maxwell's fish-eye lens.

### III. DUPLEX MIKAELIAN LENS AND DUPLEX MAXWELL'S FISH-EYE LENS

Since the gradient refractive index of different Mikaelian lenses along the  $y$  axis are all one, we splice two half-Mikaelian lenses with different real number indexes  $\{p\}$  and  $\{q\}$  to make a duplex Mikaelian lens with  $\{p, q\}$ ; see the half-Mikaelian lens with  $\{p = 2\}$  on the left and the half-Mikaelian lens with  $\{q = 1\}$  on the right in Fig. 2(a). It is clear that the gradient refractive index of a duplex Mikaelian lens with  $\{p, q\}$  does not have discrete mirror symmetry of the  $y$  axis. Derivatives of the gradient refractive index of the Mikaelian lens are written as

$$\partial_x n(x) = -\operatorname{sech}(px/a) \tanh(px/a)p/a, \quad \partial_y n(x) = 0, \quad (5)$$

where the value at the  $y$  axis is zero. Therefore, the gradient refractive index and its derivatives of the duplex Mikaelian lens are both continuous. When light rays pass through the  $y$  axis, they can be welded together smoothly, as shown by the focusing points of the  $y$  axis in Fig. 2(a). Each half of the Mikaelian lens contributes half a period to the duplex Mikaelian lens. Hence, the period of the duplex Mikaelian lens with  $\{p, q\}$  is  $L_D = L/2/p + L/2/q$  along the  $y$  axis, which is no longer the period of Mikaelian lens with  $\{p\}$  or that with  $\{q\}$ . Such a duplex Mikaelian

lens with  $\{p, q\}$  can also have a self-focusing effect, as shown in Fig. 2(a), which is a different kind of AOI. There are infinite combinations of duplex Mikaelian lenses with asymmetric gradient refractive indexes.

Is an exponential conformal transformer of a duplex Mikaelian lens with any two different real numbers,  $\{p, q\}$ , an AOI? The answer is no. Only an exponential conformal transformer of a duplex Mikaelian lens with two rational numbers  $\{p, q\} = \{p_u/p_d, q_u/q_d\}$  ( $p_u, p_d, q_u$ , and  $q_d$  are all coprime) is an AOI. We would like call such a transformer the duplex Maxwell's fish-eye lens with rational number  $\{p, q\}$ . Let us explain the reason based on exponential conformal mapping in Eq. (2). From the previous discussion, it would be much easier if we were to start from the duplex Mikaelian lens with  $\{p_u/p_d, q_u/q_d\}$ . Its period,  $L_D = \pi a p_d/p_u + \pi a q_d/q_u$ , and the reference period length,  $L = 2\pi a$ , are two important lengths for the properties of duplex Mikaelian lenses. One can find a large period of  $L_{Dg} = (p_u q_d + p_d q_u)L = 2p_u q_u L_D$ , which is  $p_u q_d + p_d q_u$  times  $L$  and  $2p_u q_u$  times  $L_D$ . Therefore, in the region of a large period,  $L_{Dg}$ , light rays from one point source have  $2p_u q_u$  periods in the duplex Mikaelian lens, which correspond to winding around the original point of the exponential conformal transformer  $p_u q_d + p_d q_u$  times and then recovering to the original propagation condition.

Let us see an example in Figs. 2(a) and 2(b) with  $\{p = p_u/p_d = 2/1\}$  and  $\{q = q_u/q_d = 1/1\}$ . In the region of a large period,  $L_{Dg}$ , between two purple solid lines, there are three periods of the reference lengths and four periods of the duplex Mikaelian lens. Such three periods of the reference lengths can be mapped to the Riemann surface between two purple solid lines in Fig. 2(b), which can be further projected to one complex plane in Fig. 2(c). Light rays in Figs. 2(b) and 2(c) wind three times around the center, while they travel back and forth along the black line four times. In this way, such a duplex Maxwell's fish-eye lens with rational number indexes can result in perfect imaging, which makes them AOIs. The light rays from a red point source at position coordinate  $(0, 0)$  can self-focus in such a duplex Mikaelian lens along the  $y$  axis; see the blue and red lines in Fig. 2(a). It should be noted that light rays from a point source located at any point can make one more image during one period of a Mikaelian lens. However, in a duplex Mikaelian lens, light rays from a point source off the  $y$  axis cannot make another image during its period (we will show this in Sec. IV). After exponential conformal mapping, the duplex Mikaelian lens becomes a different type of AOI, as shown in Fig. 2(c), which is the projection of the Riemann surface of Fig. 2(b) onto a complex plane. This type of AOI is a duplex Maxwell's

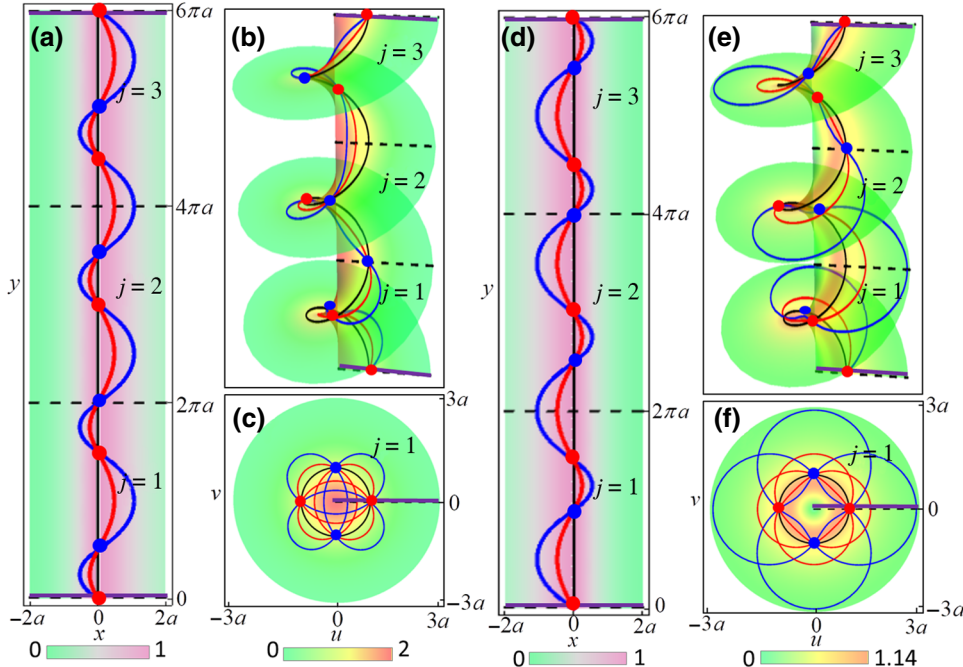


FIG. 2. Gradient refractive index and light trajectories in the duplex Mikaelian lens with  $\{p, q\}$  and the corresponding duplex Maxwell's fish-eye lens. (a) Mikaelian lens with  $\{2, 1\}$  in  $z$  space. Its gradient refractive index is without mirror symmetry along the  $y$  axis, as shown with the contour plot. During the reference period length  $L = 2\pi a$ , two red and blue light rays launch from the red source at position coordinate  $(0, 0)$  in the region marked with  $j = 1$ , which can make two more images. (b) Schematic plot of the Riemann surface and light trajectories of the duplex Maxwell's fish-eye lens with  $\{2, 1\}$ . (c) Projection to  $w$  space of the Riemann surface of (b). (d) Mikaelian lens with  $\{1, 2\}$  in  $z$  space. (e) Schematic plot of the Riemann surface and light trajectories of the duplex Maxwell's fish-eye lens with  $\{1, 2\}$ . (f) Projection to  $w$  space of the Riemann surface of (e).

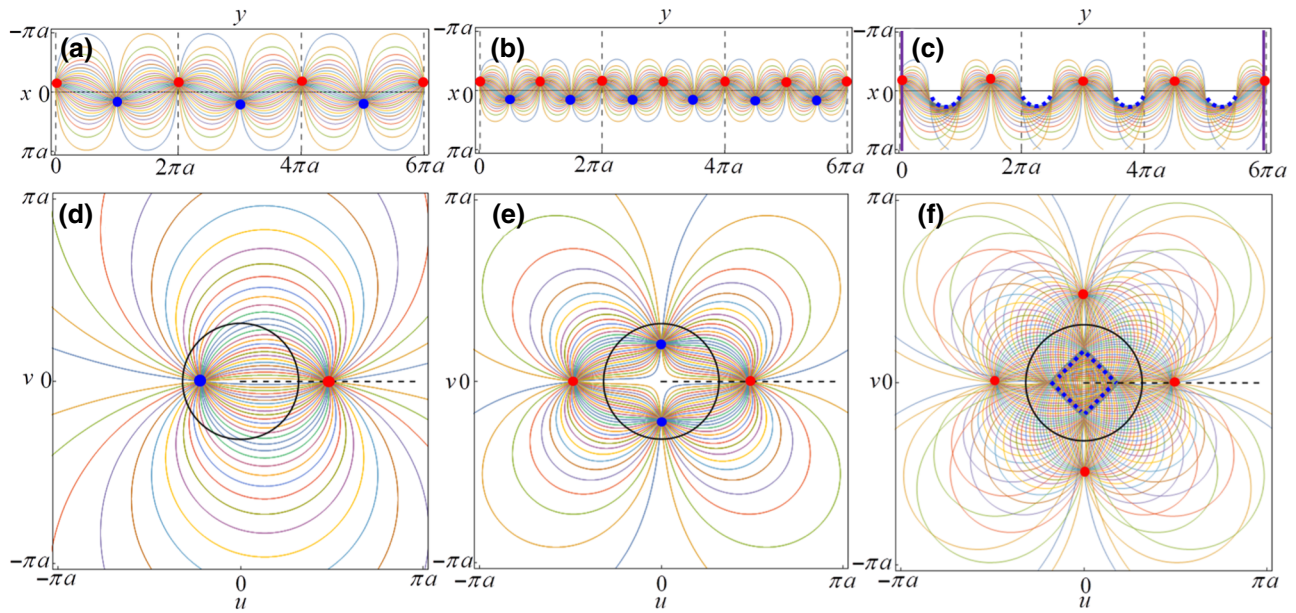


FIG. 3. (a) Colored light rays in the Mikaelian lens with  $\{p = 1\}$  emitted from and focused on red and blue points, which are off the  $y$  axis. (b) Colored light rays in the Mikaelian lens with  $\{p = 2\}$  emitted from and focused on red and blue points, which are off the  $y$  axis. (c) Colored light rays in the duplex Mikaelian lens with  $\{p = 2, q = 1\}$  emitted from and focused on red points, which are off the  $y$  axis. Blue dashed curves denote caustic curves. (d) Colored light rays in the Maxwell's fish-eye lens with  $\{p = 1\}$  emitted from and focused on red and blue points, which are off radius  $a$ . (e) Colored light rays in the Maxwell's fish-eye lens with  $\{p = 2\}$  emitted from and focused on red and blue points, which are off radius  $a$ . (f) Colored light rays in the duplex Maxwell's fish-eye lens with  $\{p = 2, q = 1\}$  emitted from and focused on red points, which are off radius  $a$ . Blue dashed squarelike curves denote caustic curves.

fish-eye lens with two rational numbers,  $\{p, q\}$ , where  $p$  is the index inside the circular region of radius  $a$  and  $q$  is outside it. Perfect imaging will also be valid in this lens, as shown by the red and blue closed trajectories and focusing points in Fig. 2(c). If two half-Mikaelian lenses in Fig. 2(a) exchange their positions, we can obtain another duplex Mikaelian lens with two rational numbers,  $\{q, p\}$ , in Fig. 2(d). The exponential conformal transformer is shown in Figs. 2(e) and 2(f). Although the duplex Mikaelian lens with  $\{p, q\}$  and duplex Mikaelian lens with  $\{q, p\}$  are similar under mirror reflection [cf. Figs. 2(a) and 2(d)], their exponential conformal transformers are quite different in their gradient refractive indexes [cf. Figs. 2(c) and 2(f)].

As for the duplex Mikaelian lens without two rational number indexes, there is no way to find a large period; hence, there is no corresponding duplex Maxwell's fish-eye lens. Therefore, we have two kinds of AOIs: one is the duplex Mikaelian lens with any two different positive real numbers  $\{p, q\}$ , and the other is the duplex Maxwell's fish-eye lens with rational number  $\{p, q\}$ .

#### IV. CAUSTICS IN DUPLEX MIKAELIAN LENSES AND DUPLEX MAXWELL'S FISH-EYE LENSES

In this section, we systematically investigate the properties of the duplex Mikaelian lens and duplex Maxwell's

fish-eye lens in terms of geometric optics. For a Mikaelian lens with  $\{p = 1\}$ , there will be two focusing points for a reference period of  $L$ , as shown in Fig. 3(a). For a better illustration, we rotate Fig. 3(a) clockwise by  $\pi/2$ , corresponding to Fig. 1(a). For a Mikaelian lens with  $\{p = 2\}$ , there will be four focusing points for a reference period of  $L$ , as shown in Fig. 3(b). After merging into a duplex Mikaelian lens with  $\{p = 1, q = 2\}$ , there will be one focusing point and one caustic curve in a period of the duplex Mikaelian lens shown in Fig. 3(c), which is also mentioned in Sec. III. The caustic of optics can be defined as the envelope of a system of orthotomic rays [19–22]. In Fig. 3(c), caustic curves are marked with blue dashed lines, where light rays will be converged along a particular curve. If the red source is approaching the  $y$  axis, the blue dashed caustics become smaller as well approaching the  $y$  axis. Once the red source is on the  $y$  axis, as shown in Fig. 2(a), the blue dashed caustics shrink to blue points. Those caustics can be treated as remnants of imaging points on the other side of the  $y$  axis due to the asymmetric gradient refractive index. Such a caustic effect will be very obvious in the corresponding duplex Maxwell's fish-eye lens after exponential conformal mapping. For the Maxwell's fish-eye lens with  $\{p = 1\}$ , the colored light rays from a source point (in red) at position coordinate  $(1.5a, 0)$  outside radius  $a$  can make a perfect image point (in blue) inside, as shown in Fig. 3(d). Including the source (or

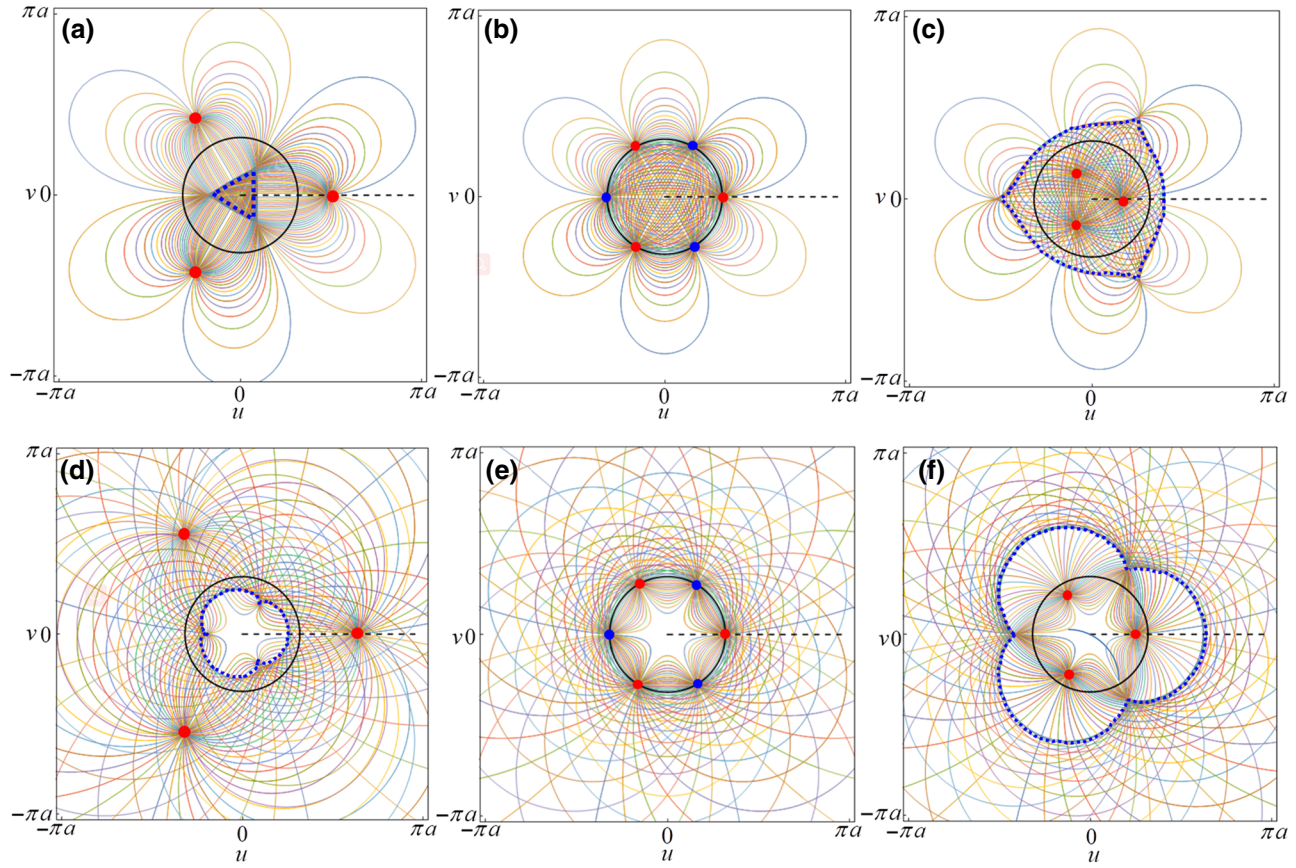


FIG. 4. (a) Colored light rays in the duplex Maxwell's fish-eye lens with  $\{p = 3, q = 1\}$  emitted from and focused on red points, which are outside radius  $a$ . Blue dashed triangularlike curve inside radius  $a$  is caustic curve. (b) Colored light rays in the duplex Maxwell's fish-eye lens with  $\{p = 3, q = 1\}$  emitted from and focused on red and blue points, which are on radius  $a$ . (c) Colored light rays in the duplex Maxwell's fish-eye lens with  $\{p = 3, q = 1\}$  emitted from and focused on red points, which are inside radius  $a$ . Blue dashed triangularlike curve outside radius  $a$  is the caustic curve. (d) Colored light rays in the duplex Maxwell's fish-eye lens with  $\{p = 1, q = 3\}$  emitted from and focused on red points, which are outside radius  $a$ . Blue dashed clover-shaped curve inside radius  $a$  is the caustic curve. (e) Colored light rays in the duplex Maxwell's fish-eye lens with  $\{p = 1, q = 3\}$  emitted from and focused on red and blue points, which are on radius  $a$ . (f) Colored light rays in the duplex Maxwell's fish-eye lens with  $\{p = 1, q = 3\}$  emitted from and focused on red points, which are inside radius  $a$ . Blue dashed clover-shaped curve outside radius  $a$  is the caustic curve.

self-image) point, there will be four imaging points (in red and blue) in the Maxwell's fish-eye lens with  $\{p = 2\}$  [see in Fig. 3(e)]. After combination, there will be four images (in red) outside radius  $a$ , as shown in Fig. 3(f). The image number is exactly the number of  $2p_uq_u$  (here, 4). The four caustic curves in Fig. 3(c) are now mapped to a squarelike caustic curve inside radius  $a$  of Fig. 3(f). If the red source is approaching radius  $a$ , as shown in Fig. 2(f), the blue dashed caustics shrink to blue points, which will overlap with the red points.

To enhance visualization of the above effect, we consider a duplex Maxwell's fish-eye lens with  $\{p = 1, q = 3\}$  in Figs. 4(a)–4(c). In Fig. 4(a), the light rays from the point source (in red) with position coordinate  $(1.5a, 0)$  will generate two more red images. Inside the radius  $a$ , there is a triangularlike caustic curve. While the red point source is approaching radius  $a$ , the triangularlike caustic

curve shrinks to three blue points, as shown in Fig. 4(b). Therefore, it has six images (three red points and three blue points) at radius  $a$ . When the red light source is placed with position coordinate  $(0.5a, 0)$  inside radius  $a$ , the triangular caustic curve is located outside [blue dashed curve in Fig. 4(c)]. The evolution of the caustic curve in a duplex Maxwell's fish-eye lens with  $\{p = 3, q = 1\}$  is plotted in Figs. 4(d)–4(f). In Fig. 4(d), the red point source is located at position coordinate  $(2a, 0)$ , and there will be two more red images outside radius  $a$ , with a clover-shaped caustic curve inside radius  $a$ . After moving the red point source to radius  $a$ , as shown in Fig. 4(e), the clover-shaped caustic curve shrinks to blue points. With the red source point placed at  $(0.8a, 0)$ , the clover-shaped caustic curve is located outside, as shown in Fig. 4(e).

As long as the ratio of  $p$  and  $q$  is a rational number, the imaging and caustic effect are still valid. However, if

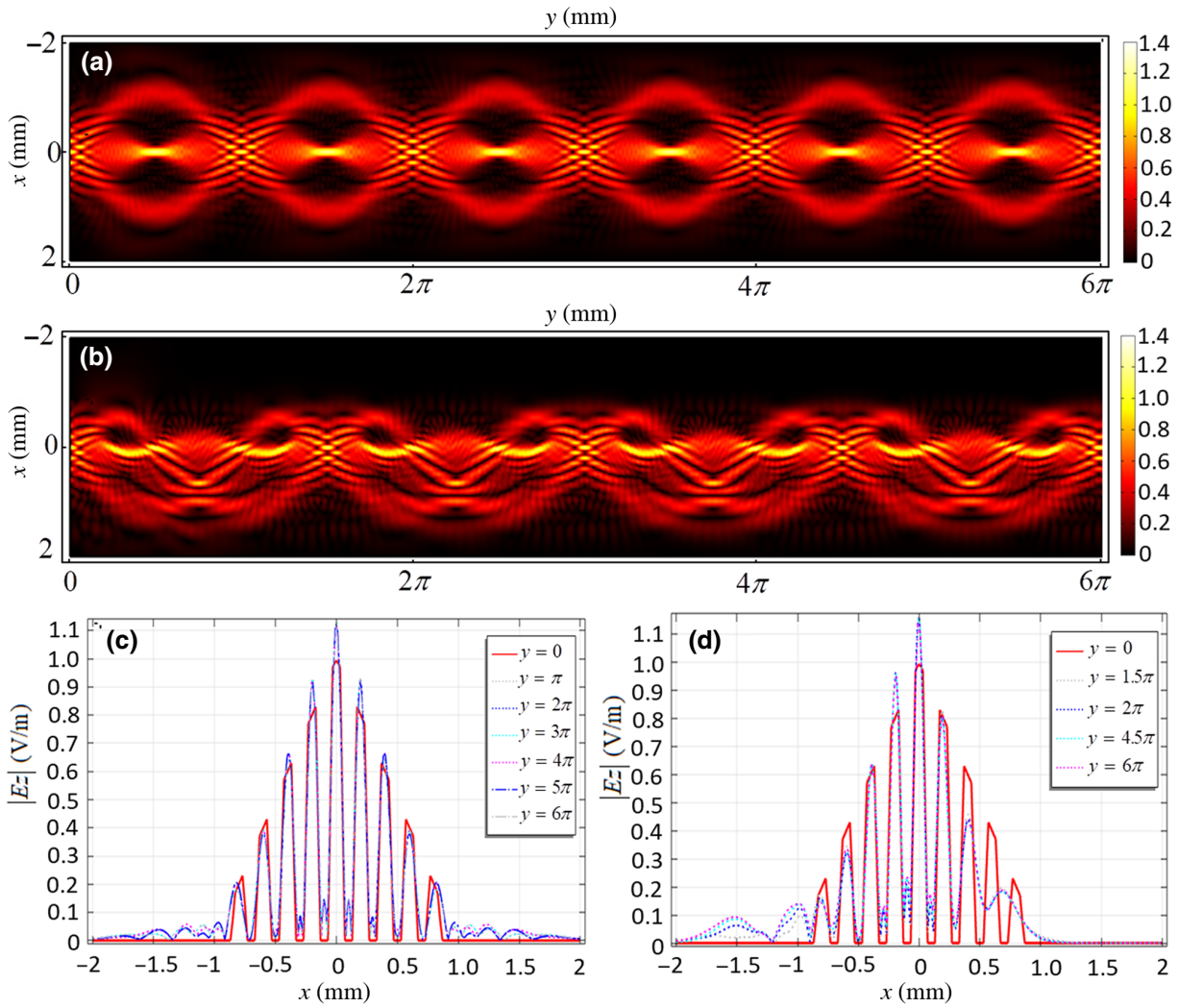


FIG. 5. Talbot effect in the Mikaelian lens and duplex Mikaelian lens. (a) Normal value of electromagnetic field  $|E_z|$  (with units of V/m) out of the plane plotted in the Mikaelian lens of Fig. 1(a). (b) Electromagnetic field plotted in the duplex Mikaelian lens of Fig. 2(a). Metallic grating source with its magnitude satisfying  $\text{abs}(1 - y)$  is set at the  $x$  axis. (c) Electromagnetic field out of the plane at every half period in the Mikaelian lens. (d) Electromagnetic field out of the plane at every period in the duplex Mikaelian lens.

the ratio becomes an irrational number, there will be no perfect imaging, similar to the effect reported in Ref. [23], and hence, the caustic effect disappears.

## V. TALBOT EFFECT IN DUPLEX MIKAELIAN LENSES

In this section, we focus on the properties of the duplex Mikaelian lens in terms of wave optics. The following full-wave simulations are performed by the rf module of the commercial software COMSOL Multiphysics. It has been demonstrated theoretically and experimentally that the Talbot effect exists in the Mikaelian lens [14]. The Talbot effect is the self-imaging of a grating in an optical system, when it is illuminated by a monochromatic plane wave [24–27]. In Fig 5(a), array sources with their electric component out of the plane of the electromagnetic wave

(with frequency 1 THz,  $a = 1$  mm), satisfying  $\text{abs}(1 - y)$ , are placed in the metallic grating along the  $x$  axis of the Mikaelian lens with  $\{p = 2\}$ . Here, we also rotate Fig. 5(a) clockwise by  $\pi/2$ . We plot their electric component at every half period of  $L_0/2 = \pi$  in Fig. 5(c). It shows the Talbot effect of the wave phenomenon, where the image pattern of array sources can reappear at every half period. For the duplex Mikaelian lens with  $\{p = 2, q = 1\}$  of Fig. 2(a), we plot the electric field in Fig. 5(b), which is under the same metallic grating source setting as that of Fig. 5(a). The electric component at every period  $L_D$  is plotted in Fig. 5(d), which demonstrates the Talbot effect in this duplex Mikaelian lens. The main difference between the two Talbot effects is that their periods and the symmetry of the field profile are different, which comes from the mirror symmetry of the Mikaelian lens and asymmetry of the duplex Mikaelian lens. In wave optics, duplex Mikaelian

lenses and their exponential conformal transformers are not equivalent, and this deserves further investigation.

## VI. CONCLUSION

We report two kinds of AOIs in 2D space. One is the duplex Mikaelian lens with any two different positive real numbers  $\{p, q\}$ , resulting from continuous translation symmetry described by the Lie group  $R^1$ . The other is a duplex Maxwell's fish-eye lens with rational number  $\{p, q\}$  because of its continuous rotation symmetry described by the Lie group  $S^1$ . A heuristic explanation is given based on exponential conformal mapping. Owing to the asymmetric gradient refractive index, the caustic effect of geometric optics is shown in duplex Mikaelian lenses and duplex Maxwell's fish-eye lenses by means of a ray-tracing method. The Talbot effect of wave optics is also demonstrated in duplex Mikaelian lenses with numeric simulations. Our results enhance the family of AOIs and their imaging properties. These AOIs should also have counterparts in surface plasmons, acoustics, and so on, and hence, might result in applications based on asymmetric gradient refractive indexes.

## ACKNOWLEDGMENTS

This work is financially supported by the National Natural Science Foundation of China (Grants No. 11874311 and No. 11904006), National Science Foundation of Anhui Province of China (Grant No. 1908085QA20), and the Recruitment Program for Leading Talent Team of Anhui Province (2019-16). We thank the support from Professor Zhong Chen, Professor Huiqiong Wang, Professor Yinshui Fang, Mr. Jingfeng Chen, Miss Yuling Zheng, Mr. Jian-qing Zhou, Miss Shanshan Lin, Miss Sichen Tao, Miss Ying Chen, Mr. Shan Zhu, and Mr. Pengfei Zhao.

S. Liu, Y. Wu, Y. Yan, and Z. Zhou are undergraduate students at Xiamen University Malaysia.

- [1] M. Born and E. Wolf, *Principles of Optics: Electromagnetic Theory of Propagation, Interference and Diffraction of Light* (Cambridge University Press, Cambridge, England, 2006).
- [2] J. L. Synge, The absolute optical instrument, *Trans Am. Math. Soc.* **44**, 32 (1938).
- [3] R. K. Luneburg and M. Herzberger, *Mathematical Theory of Optics* (University of California Press, Berkeley and Los Angeles, 1964).
- [4] J. C. Miñano, Perfect imaging in a homogeneous three-dimensional region, *Opt. Express* **14**, 9627 (2006).
- [5] U. Leonhardt, Perfect imaging without negative refraction, *New J. Phys.* **11**, 093040 (2009).
- [6] T. Tyc, L. Herzánová, M. Šarbort, and K. Bering, Absolute instruments and perfect imaging in geometrical optics, *New J. Phys.* **13**, 115004 (2011).
- [7] T. Tyc and A. J. Danner, Absolute optical instruments, classical superintegrability, and separability of the Hamilton-Jacobi equation, *Phys. Rev. A* **96**, 053838 (2017).
- [8] L. Xu and H. Chen, Coherent perfect absorber makes a perfect drain for Maxwell's fish-eye lens, *Europhys. Lett.* **100**, 34001 (2012).
- [9] T. Tyc and A. Danner, Resolution of Maxwell's fisheye with an optimal active drain, *New J. Phys.* **16**, 063001 (2014).
- [10] U. Leonhardt and S. Sahebdivan, Theory of Maxwell's fish eye with mutually interacting sources and drains, *Phys. Rev. A* **92**, 053848 (2015).
- [11] L. Xu and H. Chen, Conformal transformation optics, *Nat. Photonics* **9**, 15 (2015).
- [12] L. Xu, H. Chen, T. Tyc, Y. Xie, and S. A. Cummer, Perfect conformal invisible device with feasible refractive indexes, *Phys. Rev. B* **93**, 041406(R) (2016).
- [13] L. Xu, T. Tyc, and H. Chen, Conformal optical devices based on geodesic lenses, *Opt. Express* **27**, 28722 (2019).
- [14] X. Wang, H. Chen, H. Liu, L. Xu, C. Sheng, and S. Zhu, Self-Focusing and the Talbot Effect in Conformal Transformation Optics, *Phys. Rev. Lett.* **119**, 033902 (2017).
- [15] A. L. Mikaelian and A. M. Prokhorov, V self-focusing media with variable index of refraction, *Prog. Opt.* **17**, 279 (1980).
- [16] U. Leonhardt and T. Philbin, *Geometry and Light: the Science of Invisibility* (Dover Inc., Mineola, New York, 2010).
- [17] U. Leonhardt, Optical conformal mapping, *Science* **312**, 1777 (2006).
- [18] Y. N. Demkov and V. Ostrovsky, Internal symmetry of the Maxwell "fish-eye" problem and the Fock group for the Hydrogen atom, *Sov. Phys. JETP* **33**, 1083 (1971).
- [19] O. N. Stavroudis, *The Mathematics of Geometrical and Physical Optics: the k-Function and its Ramifications* (Wiley-VCH, Weinheim, Germany, 2006).
- [20] M. Marciano-Melchor, E. Montiel-Piña, E. Román-Hernández, A. Rosado, J. G. Santiago-Santiago, G. Silva-Ortigoza, R. Silva-Ortigoza, and R. Suárez-Xique, Wavefronts, light rays and caustic of a circular wave reflected by an arbitrary smooth curve, *J. Opt.* **13**, 055705 (2011).
- [21] S. Maca-García, M. Avendaño-Alejo, and L. Castañeda, Caustics in a meridional plane produced by concave conic mirrors, *J. Opt. Soc. Am. A Opt. Image Sci. Vis.* **29**, 1977 (2012).
- [22] H. Y. Peng and H. Y. Chen, Caustics From Optical Conformal Mappings, *Phys. Rev. Appl.* **12**, 064030 (2019).
- [23] H. Chen, Imaging along conformal curves, *Phys. Rev. A* **98**, 043843 (2018).
- [24] H. F. Talbot, LXXVI. Facts relating to optical science. No. IV, London, Edinburgh Dublin Philos. Mag. J. Sci. **9**, 401 (1836).
- [25] L. Rayleigh, XXV. On copying diffraction-gratings, and on some phenomena connected therewith, London, Edinburgh Dublin Philos. Mag. J. Sci. **11**, 196-205 (1881).
- [26] J. Cowley and A. Moodie, Fourier images: I-the point source, *Proc. Phys. Soc. London, Sect. B* **70**, 486 (1957).
- [27] C. Zhou, W. Wang, E. Dai, and L. Liu, The talbot effect, *Opt. Photonics News*, **15**, 46 (2004).